ADVANCED MATERIALS INTERFACES

www.advmatinterfaces.de

Nanogenerators Begin to Light Up: A Novel Poling-Free Piezoelectric System with Multicolor Photoluminescence as an Efficient Mechatronics Development Platform

Songyuan Ma, Long Jin, Xi Huang, Christos Riziotis, Rui Huang, Chaoliang Zhang, Jun Lu, and Weiqing Yang**

In this work, a novel design of poly (vinylidene fluoride)/carbon quantum dots (PVDF/CQDs) based flexible poling-free hybrid material system able to efficiently convert small amounts of mechanical energy into electricity through the intrinsic piezoelectric nanostructures is reported. The PVDF/CQDs composite is fabricated through solution casting followed by a high-pressure crystallization process. The introduction of 3D quasi-spherical CQDs has in situ induced the self-assembly of polymorphic substructures in the PVDF crystallites at high pressure, and piezoelectric 3D nanosheet arrays, 1D nanometer small sticks, and 1D nanowires, respectively, are formed in situ with the increase of CQDs concentration. Without any electrical polarization treatment, the maximum open-circuit voltage output density of the durable composite system reaches 19.2 V cm^{-2} and short-circuit current output density of 550 nA cm^{-2}, both far exceeding that of pure PVDF. Simultaneously, owing to the successful incorporation of CQDs, the material shows excellent fluorescent effect with high stability, and its multicolor photoluminescence is well retained even after the endurance for a rigorous treatment at high pressure and high temperature. The as-developed environmental friendly PVDF/CQDs compound may diversify niche applications in a new-generation of self-powered autonomous optoelectronic devices, biosensors, cell imaging, and so on.

1. Introduction

Clean energy production is one of the most demanding problems we are facing today. Since the dependence upon fossil fuels must be cut down for the well-known environmental restrictions and latest guidelines, scientists have been focusing on the utilization of wide-ranging renewable energy. An enlightening idea has arisen over the latest publications to harvest environmental energy through employment of various piezoelectric, pyroelectric, and triboelectric materials.[1,2] Thereinto, piezoelectric materials, possessing the ability to capture mechanical energy with different amplitudes and frequencies, have been intensively developed to harvest energy from the ambient environment.[3,4] Energy harvesting is becoming a major technological trend not only for pure and clean energy production but equal importantly for aiding the development of energy autonomous monitoring systems like large area wireless access networks[5] or body wearable sensors that form key parts of the future Internet of Things ecosystem. Piezoelectric materials act as energy transducers through generating charges on the surfaces in response to an applied force.[6] In the past reports, ZnO nanowires were considered to be the excellent materials for developing nanogenerators compared with other traditional piezoelectric materials. Nonetheless, drawbacks to the prevalent application of ZnO nanowire materials are obvious too, such as the relatively low piezoelectric coefficient.[7] Furthermore widely used piezo-ceramic materials, despite their mechanical robustness and relatively high electromechanical coupling coefficient, exhibit also certain intrinsic major drawbacks such as limited mechanical flexibility, high fragility, and usually high content

S. Ma, L. Jin, X. Huang, Prof. J. Lu,[+] Prof. W. Yang
Key Laboratory of Advanced Technologies of Materials
Ministry of Education
School of Materials Science and Engineering
Southwest Jiaotong University
Chengdu, 610031 Sichuan, China
E-mail: junluprc@hotmail.com; wqyang@swjtu.edu.cn

The ORCID identification number(s) for the author(s) of this article can be found under https://doi.org/10.1002/admi.201800587.

[+]Other used names Jun Lv and Jun Lyu.

DOI: 10.1002/admi.201800587

Dr. C. Riziotis
Theoretical & Physical Chemistry Institute
National Hellenic Research Foundation
Athens 11635, Greece

Prof. R. Huang
College of Polymer Materials Science and Engineering
Sichuan University
Chengdu, 610065 Sichuan, China

C. Zhang
State Key Laboratory of Oral Diseases
West China Hospital of Stomatology
Sichuan University
Chengdu 610041, China

of heavy metals limiting thus their potential use in an environmentally viable way in large area harvesting devices. Therefore, it is desirable to explore more suitable, efficient and ecofriendly material systems for the development of more advanced devices[7,8] based on generators with various nanostructures as flexible energy collectors.[9]

Poly (vinylidene fluoride) (PVDF) is favored for its finer performance, such as good mechanical property, chemical and fatigue resistance, excellent piezoelectric and ferroelectric properties, form flexibility, processing simplicity and, all in all, PVDF-based nanogenerators possess rather high piezoelectric coefficients.[10–12] In previous works, numerous studies have been conducted on energy harvesting from aperiodic and irregular mechanical forces, including respiration, body movement, solid pressure, and airflow and converting them into electricity by virtue of piezoelectric materials. These energy sources, collected by all means, have demonstrated usage in powering light-emitting diodes, liquid-crystal displays, self-powered piezoionic strain sensors, and many implantable and biocompatible pressure sensors which are implemented on a catheter for minimally invasive surgery.[1,13,14] The sensors could be directly attached to human skin, monitor physiological states, and give feedback of the body in real time, thus displaying essential features, i.e., pressure-sensing capabilities, for the next generation of smart embedded and autonomous systems.[14,15] Self-powered nanosystem that harvests its operating energy from the ambient environment stably and efficiently is an attractive approach as integration platform for sensing, suggesting an emerging field in nanoenergy.[16] Successful development of PVDF-based piezoelectric devices depends on the effective fabrication of polar crystalline structures, such as the β phase structure. Among the different kinds of methods to induce polar β form in PVDF matrix, including drawing under certain temperature, electrospinning, and application of high electric filed, high-pressure-crystallized PVDF tends to have less defects and higher degree of crystallization.[12,17–19]

Quantum dots (QDs) generally refer to the nanoscale particles subject to the quantum-confinement effect, which appear as core components in many photonics platforms finding numerous applications in sensing imaging, single photon sources for quantum applications, and other fields.[20] Compared with metal-based QDs such as CdSe and CdTe and the raising concern over their environmental toxicity, biocompatibility, and stability,[21] carbon quantum dots (CQDs), also called carbon nanodots, not only could avoid these problems by nature, but also exhibit unique and tunable photoluminescent and optical properties, nanoscale aqueous solubility, special physical and chemical properties, etc.,[22] thus leading to a bright future for their applications in environmental engineering, bioimaging as well as medical treatment.[23] CQDs are structurally distinct from graphene quantum dots (GQDs).[22–24] The former are 3D quasi-spherical nanoparticles usually <10 nm in diameter, and the later are 2D fragments of single or a few layered graphene, with lateral dimensions larger than their height.[22–24]

Herein, we intend to design and fabricate a novel PVDF/CQDs-based piezoelectric photoluminescent composite system. The PVDF/CQDs composites were prepared by solution casting followed by a high-pressure crystallization process. Multiform piezoelectric nanostructures were observed in the high-pressure-crystallized composite samples with different component ratios, including 3D nanosheet arrays, 1D nanometer small sticks, and 1D nanowires, depending on CQDs concentration. Without any electrical poling treatment, these in situ formed nanostructures could efficiently convert small amounts of mechanical energy into electricity by their intrinsic piezoelectricity, and the measured electrical output density exceeded that of most of state-of-the-art piezopolymers reported to date. Together with the multicolor photoluminescent effect introduced by CQDs, the compound material exhibits interesting photoelectric properties and presents potential applications in advanced photonics, biomedical device, imaging, environmental monitoring, and other related high-tech fields by exploiting also the flexibility of variable length scale production, from microscale to large-scale mechatronic systems.

2. Results and Discussion

Figure 1 and **Table 1** show the differential scanning calorimetry (DSC), wide angle X-ray diffraction (WAXD), and attenuated total reflectance Fourier transform infrared spectroscopy (ATR-FTIR) testing results of the PVDF/CQDs composites with different concentrations of CQDs, prepared through

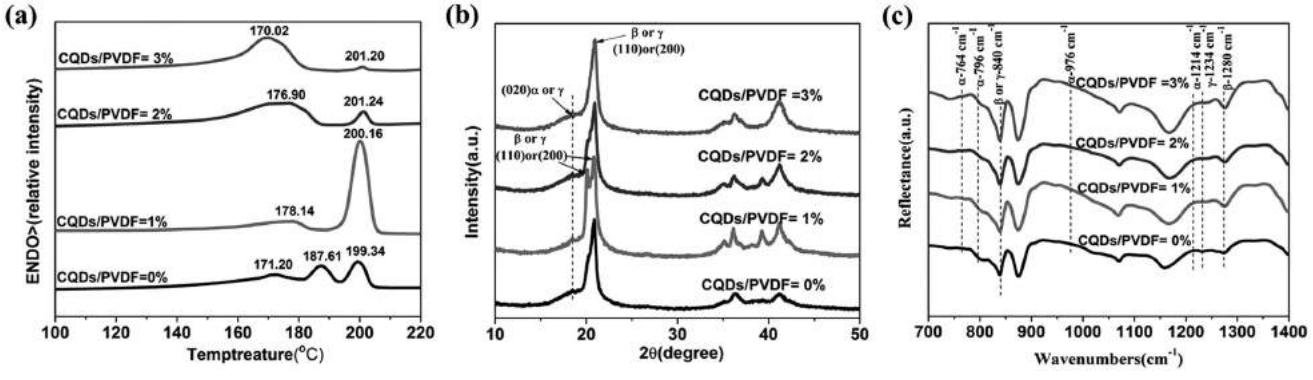

Figure 1. DSC a), WAXD b) and ATR-FTIR c) graphs of the PVDF/CQDs composite samples with different contents of CQDs, crystallized at 400 MPa, 260 °C for 10 min.

Table 1. Absolute contents of α, β, and γ phase crystals in various PVDF/CQDs samples crystallized at 400 MPa, 260 °C for 10 min, calculated from Equations (1)–(4).

Sample	CQDs [%]	α [%]	β [%]	γ [%]
$PVDF_{100}/CQD_0$	0	0.12	58.18	11.63
$PVDF_{99}/CQD_1$	1	0.08	83.67	4.69
$PVDF_{98}/CQD_2$	2	0	63.33	0.19
$PVDF_{97}/CQD_3$	3	0	63.78	0.12

crystallization at 400 MPa, 260 °C for 10 min. With the increase of CQDs content, the area of melting peak first increased and then decreased, reaching the maximum at PVDF/CQDs (99/1, wt/wt) (Figure 1a). This indicated that the morphology and form of PVDF crystals changed together with different contents of CQDs. Particularly, the higher melting points of the high-pressure-crystallized samples were all around 200 °C, suggesting the addition of CQDs has induced the growth of extended-chain PVDF crystals in the matrix.[11,19] The crystalline phase of PVDF in the substrate was further identified by WAXD and FTIR measurements (Figure 1b,c). Based on the X-ray diffraction pattern, apparent monolayers of superimposed orthogonal β phases from (110) and (200) reflections at 20.4–21.1° in the 2θ angle were observed in the sample. In addition, characteristic IR wavenumbers at 840 and 1280 cm^{-1} further confirmed that β phase was induced in the composite. With the increase of the content of CQDs, the fraction of β phase crystallites first increased and then decreased, and reached maximum value at PVDF/CQDs (99/1, wt/wt; Table 1). In that situation, γ phase still coexisted with β phase in the matrix, as noted in the WAXD and IR spectra.

Figure 2 shows the scanning electron microscopy (SEM) images of the etched fractured surfaces of the PVDF/CQDs samples. For the sample composed of pure PVDF (Figure 2a,b), certain extended-chain crystals, with striated appearance as the most typical feature, were observed clearly. With the increase of CQDs content, the morphology and structure of the composites were distinct from that of the homopolymer as a result of intensively grown β phase crystals on a large scale. For PVDF/CQDs (99/1, wt/wt), of which the IR absorption bands characteristic of crystalline β phase reached the maximum volume (Figure 1c), a large number of nanosheet arrays appeared in SEM image, which somewhat presented interesting micronano spherical crystal structure (Figure 2c,d). For PVDF/CQDs (98/2, wt/wt), some nanosacle sticks emerged on the crystal surface (Figure 2e,f). And for PVDF/CQDs (97/3, wt/wt), there were large numbers of crystalline nanowires mixed with rod-shaped structures (Figure 2g,h).

Based on the above diagrams, it can be concluded that polymorphic β phase crystals were obtained in the PVDF/CQDs compounds in the wake of variable CQDs content loading, including 3D nanosheet arrays, 1D nanoscale small stick structures, and 1D nanowires. Crystallization pressure, temperature, duration time, as well as component ratio are all influencing factors for the formation of β phase crystals. By purposively adjusting experimental parameters, we are able to find the perfect PVDF/CQDs composite system and make it good candidate for the fabrication of piezoelectric nanogenerators (PNGs) with outstanding electric generating performance.

The electrical output density of the poling-free PVDF/CQDs compounds, fabricated with different CQDs concentration, was measured under the stimulation of low frequency impacts. **Figure 3**a,b showed the open-circuit voltage output density and short-circuit current output density of various PVDF/CQDs samples at a stimulating frequency of 1.5 Hz and applied force of 10 N. With the increase in the content of CQDs, the voltage output density and current output density first increased and then decreased synchronously. Maximum peak values were attained from PVDF/CQDs (99/1, wt/wt), 180 nA cm^{-2} and

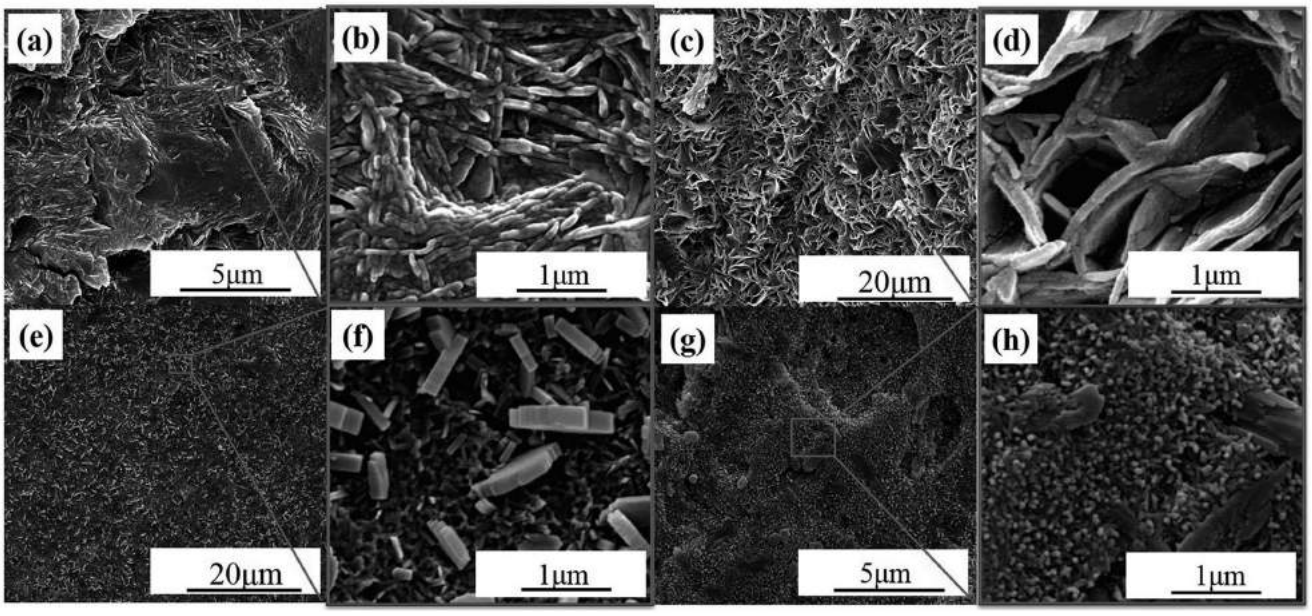

Figure 2. SEM cross-sectional view of the PVDF/CQDs composite samples with different component ratios, crystallized at 400 MPa, 260 °C for 10 min.

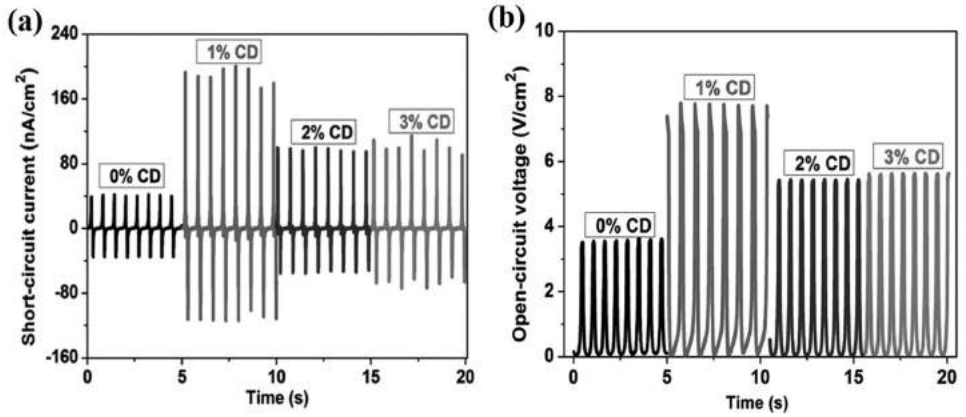

Figure 3. Short-circuit current output density a) and open-circuit voltage output density b) of the PVDF/CQDs composites with different component ratios, generated at a stimulating frequency of 1.5 Hz and applied force of 10 N.

7.6 V cm^{-2} for the short-circuit current output density and open-circuit voltage output density, respectively. Without any treatment of polarization, the material systems we developed are able to efficiently convert ambient mechanical energy into electricity for the realization of self-powered, sustainable, and environmental friendly devices.

In many references, it is difficult to give rise to macroscopic polarization in PVDF, though the existence of crystalline β phase has been achived for the polymer.[25] For bulk piezoelectric polymers, their piezoelectric effect is due mainly to the molecular structures of the polymers and their orientation.[25] The molecular structure of a piezopolymer should inherently contain molecular dipoles, and these dipoles can be reoriented and kept in their preferred orientation state.[25] In a word, there are structural requirement for a bulk piezopolymer to realize its piezoelectricity.[25] Commonly, the reorientation of the crystallites within the bulk polymer matrix is done through a poling process with the application of a high electrical field at an elevated temperature.[25] Interestingly, as shown in Figure 3, herein the pure PVDF also showed relative good piezoelectric response without any electrical polarization treatment. This should be attributed to the pressure induced growth of extended-chain crystals in the sample (Figure 2a,b). Reputed as a kind of equilibrium crystal, polymer extended-chain crystals, in which the molecular chains run parallel to each other, are with a combination of 3D crystaline ordering and long-chain molecular orientational ordering.[26] Therefore, high-pressure crystallization that resulted in the large-scale formation of β phase extended-chain lamellae played the same role as electrical poling for PVDF, and at the same time avoided its disadvantages, such as substantial additional power consumption and sometimes electrical breakdown of the samples.

Considering the DSC, WAXD, IR, and SEM characterization results, we believed that different electrical output of different component ratio systems in Figure 3 could be attributed to the variation of distribution and size of CQDs, and crystallization form, morphology, and substructures of the internally pressure-formed PVDF nanostructured crystals. 3D nanosheet arrays were formed when adding 1 wt% CQDs into the system, some 1D nanometer small stick structures with 2 wt% CQDs, and 1D nanowires when 3 wt% CQDs were added. From the point of view of short-circuit current and open-circuit voltage, the piezoelectric property of 3D nanosheet arrays should be superior to 1D nano stick structures and 1D nanowires. Besides, piezoelectric property of any PVDF/CQDs composite system should be better than that of pure PVDF. The maximum short-circuit current output density of the composites exceeded four times that of pure homopolymer, while maximum open-circuit voltage output density two times higher that of pure homopolymer. Unlike the crystalline nanostrcutures in the other samples, the nanosheets in the composite with 1 wt% CQDs were formed in an array state. Such vertically aligned array state allows the nanosheets to bend and relax more synergistically, and undergo larger deformation when the PVDF/CQDs-based devices are subject to mechanical forces. Moreover, as shown in Figure 1a and Table 1, the fraction of β phase crystals in PVDF/CQDs (99/1, wt/wt) composite is the highest, and the formed nanosheets are actually with β phase extended-chain lamellae as their substructures. Consequently, the PVDF/CQDs composite with 1 wt% CQDs concentration exhibits higher electrical conversion efficiency.

In practical applications, the collected vibration energy is often aperiodic and irregular, with inconstant amplitudes and frequencies. Hence, it is necessary to evaluate the electrical performance in a condition resembling the real world. **Figure 4** shows the electrical output density of a PVDF/CQDs (99/1, wt/wt) sample with varying frequency and applied force. The frequency and applied force were controlled by a force sensor. As can be seen from Figure 4a,b, the short-circuit current output density and open-circuit voltage output density in a stretching cycle increased with the applied force. The average short-circuit current output density was 210 nA cm^{-2} for an external force of 10 N, 250 nA cm^{-2} for an applied force of 30 N, and reached up to 300 nA cm^{-2} as the mechanical force increased to 50 N. In the meantime, the open-circuit voltage output density gradually increased from 8.2 to 15.2 V cm^{-2}. The piezoelectric response of the compound matrix was in accordance with the degree of deformation. We also tested its piezoelectric performance at different frequencies by applying a constant load of 10 N, and increased the frequency from 1. to 4.5 Hz (Figure 4c,d). It turned out the short-circuit current output density increased from 210 to 550 nA cm^{-2} and open-circuit voltage output

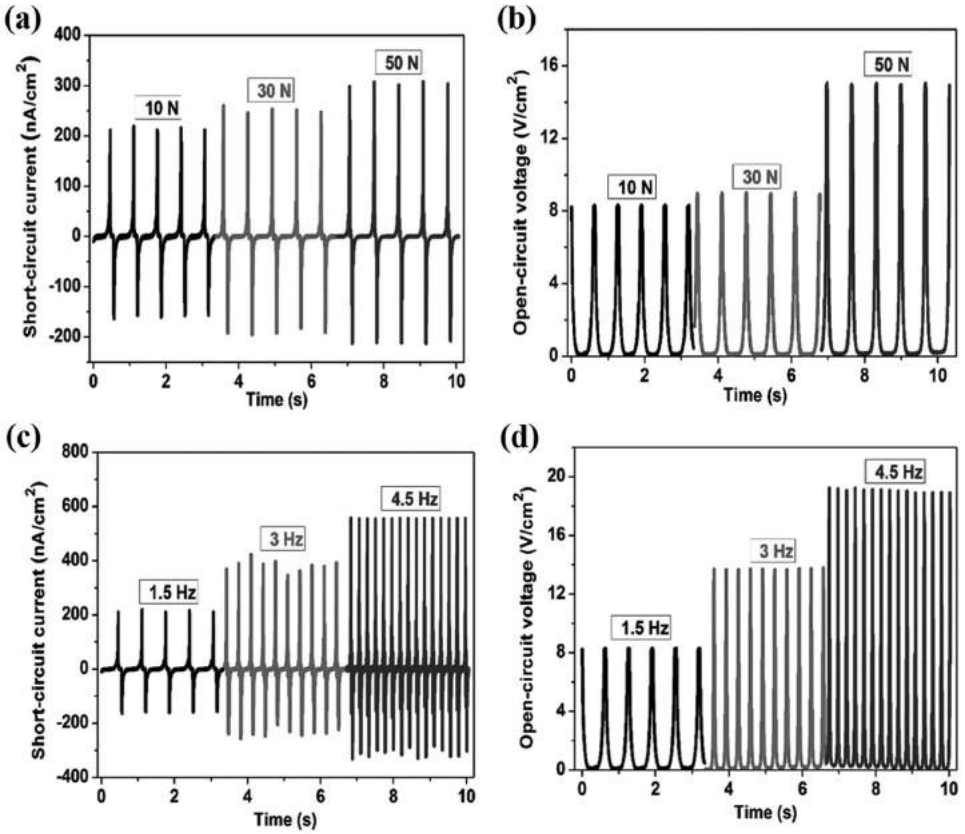

Figure 4. Electrical output density of a PVDF/CQDs (99/1, wt/wt) under various loads or frequencies: a) short-circuit current output density and b) open-circuit voltage output density were measured at a fixed frequency of 1.5 Hz; c) short-circuit current output density and d) open-circuit voltage output density were measured at a fixed force of 10 N.

density accordingly increased from 8.2 to 19.2 V cm^{-2}. For a comparison, the PVDF/CQDs composites with 2 and 3 wt% CQDs concentrations, as well as the pristine PVDF, were still tested at a fixed 1.5 Hz frequency with variant 10, 30, and 50 N forces (Figure S1, Supporting Information), and at a constant 10 N force with increased 1.5, 3 and 4.5 Hz frequencies (Figure S2, Supporting Information). Evidently, the composite with 1 wt% CQDs, in which nanosheet arrays were formed, further demonstrated the best piezoelectricity among 1–3 wt% CQDs composites, and its electrical outputs still significantly surpassed those of the pure PVDF even if the applied load and frequency have varied. Based on the above piezoelectric experiments, we may draw the conclusion that the PVDF/CQDs system exhibits excellent piezo-responsivity to the mechanical stimulus with a higher frequency, and increasing excitation or frequency stably leads to higher power output density. However, an upper frequency limit that will correspond also to maximum voltage is unable to be determined at present stage, due also to the generated frequency limit of the employed impacting test instrument.

For the successful development of piezoelectric-material-based nanogenerators, the substrates should be qualified for long-term operation, by working stably and sustainably. Herein, we chose the short-circuit current output density as the assessment parameter to characterize the stability and durability of the as fabricated PVDF/CQDs composite sample. A newly prepared PVDF/CQDs (99/1, wt/wt) composite sample continuously operated for more than 1000 cycles at a stimulated force of 50 N and frequency of 1.5 Hz, and the test result is shown in **Figure 5**. With the experimental time extended, the electrical output density kept increasing until the hits reached ≈600 cycles. This is because as time extends, the electron transmission rate increases, and charges accumulate on the surface

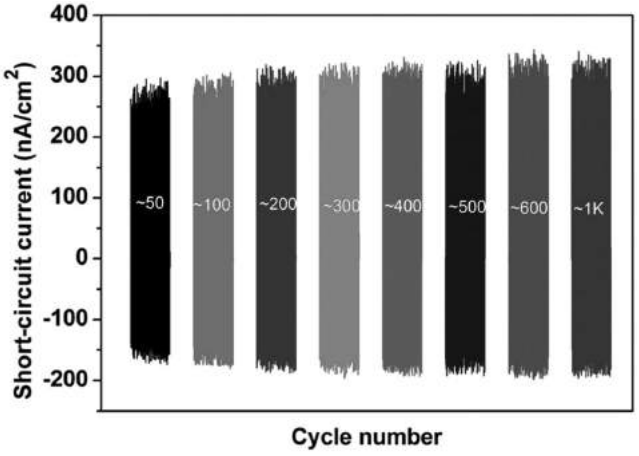

Figure 5. Stability and durability test of a PVDF/CQDs (99/1, wt/wt) sample, whole signal, stimulated by a 1.5 Hz 50 N impact.

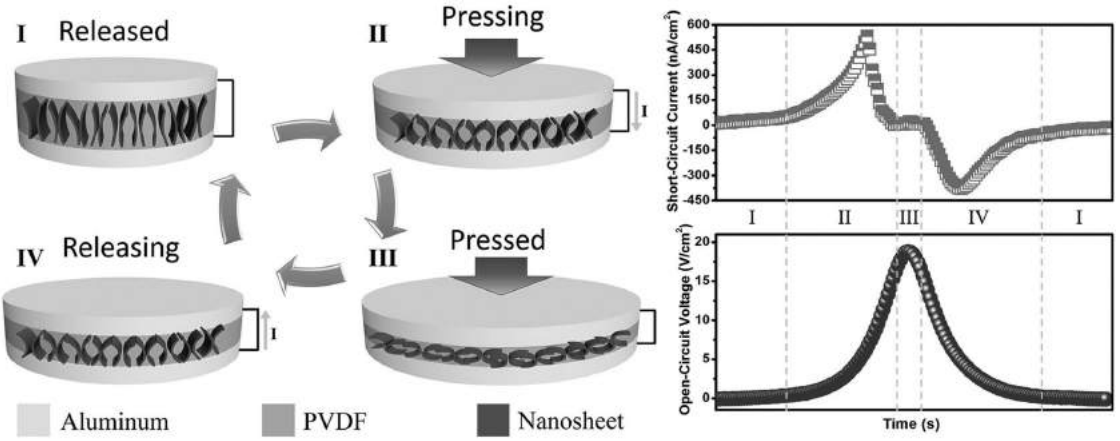

Figure 6. Schematic drawing of the composite structure and working mechanism for a PVDF/CQDs-based PNG.

to form electrets, and the piezoelectric property of the composite system is consequently improved at the initial stage. However, a balance state was achieved for the sample with the test time further increased. As can be noted, the sample attained a stable state for electrical outputs when the hits exceeded ≈600 cycles. It operated for additional ≈400 cycles with excellent performance stability and repeatability, and no electrical output decay was observed when the test was terminated.

The composite structure and working mechanism of the as-developed poling-free dynamic PNGs, for the capturing of kinetic mechanical energy, are schematically described in **Figure 6**. Its working process can be divided into four stages. The first stage is the original state without any exertion of force (Figure 6, stage I). In the second stage, when the vertical compressive force is applied on the sample, the nanosheet array structure of PVDF bends so that the voltage begins to generate on both sides of electrodes. The electrons flow from the lower electrode to the upper electrode due to the generated potential, resulting in current from the upper electrode to the lower electrode (Figure 6, stage II). The third process shows that the nanosheet array structure of the sample reaches the maximum bending state, and the voltage presents the maximum potential (Figure 6, stage III). The fourth stage is the process of releasing. The internal nanosheet array structure tends to its original shape. Therefore, piezo and voltage are changing to zero, and the electrons will flow back to the lower electrode, resulting opposite current (Figure 6, stage IV).

Figure 7 shows the LSCM images of PVDF/CQDs (99/1, wt/wt) samples before and after high-pressure processing as well as the typical PL emission spectra of the PVDF/CQDs mixtures under different excitation lights by using a fluorescence spectrometer. It can be seen clearly from the diagram that the spin-coated PVDF/CQDs film irradiated different colors under variable excitation light sources, emitting blue light under the excitation of ultraviolet light, green light under blue, yellow light under green, and red light under the excitation of red light (Figure 7a–d). Thus, the PVDF/CQDs blend has the desirable essential multicolor fluorescent property before high-pressure treatment, and this is because the luminescent effect is not only determined by the quantum size effect, but largely influenced by the surface defect and edge effect of the introduced CQDs.[22–24] However, it is still vital to learn whether the as-prepared compound still maintains this performance after a high-pressure crystallization process, as this has direct influence on its application. Fluorescence images of the pressure-treated crystalline compound sample are shown in Figure 7e–h, with testing conditions as stated before. Astonishingly, the sample presented just the same photoluminescence (PL) behavior as the spin-coated film, eradiating blue, green, yellow, and red lights at the excitations of ultraviolet, blue, green, and red lights, respectively. Therefore, it demonstrated that the PVDF/CQDs composite maintained the multicolor fluorescence properties even after the rigorous process of high-pressure and high-temperature crystallization. Moreover, the PL spectra results are consistent with the LSCM observations. From the typical emission spectra of the PVDF/CQDs (Figure 7i), it can be observed that the emission peaks centered at 439, 529, 580, and 672 nm, corresponding to the optimum excitation wavelengthes of the mixtures at 365, 468, 528, and 610 nm, respectively.

In the 1966 film "Fantastic Voyage," a submarine carrying a team of scientists is shrunk to the size of a microbe and injected into a dying man for vascular surgery. Artificial self-propelled micro/nanoscale machines, small devices capable of autonomous movement, are a powerful scientific innovation for solving various biomedical and environmental issues.[27] They have demonstrated considerable potential for performing operations and tasks in on-demand treatment and therapies for a desired duration and finally be removed without causing adverse or toxic effects.[27] Nevertheless, it is still challenging to make the synthetic functional motors on the nano- and micrometer length scales, mainly due to the difficulty in fabricating structurally complex objects of this size and scaling down of the familiar macroscopic principles of powering them.[27,28] Also, the choice of materials for the design and fabrication of the micro/nanomotors is crucial for their shape, mechanism, and propulsion efficiency.[27,28] Ideally, such biomedical machines should be self-powered in vivo by converting the numerous body-providing energy, such as biological mechanical energy and biofluid hydraulic energy.[29,30]

We have demonstrated the engineering and optimization of formation of piezoelectric polymeric nanostructures by

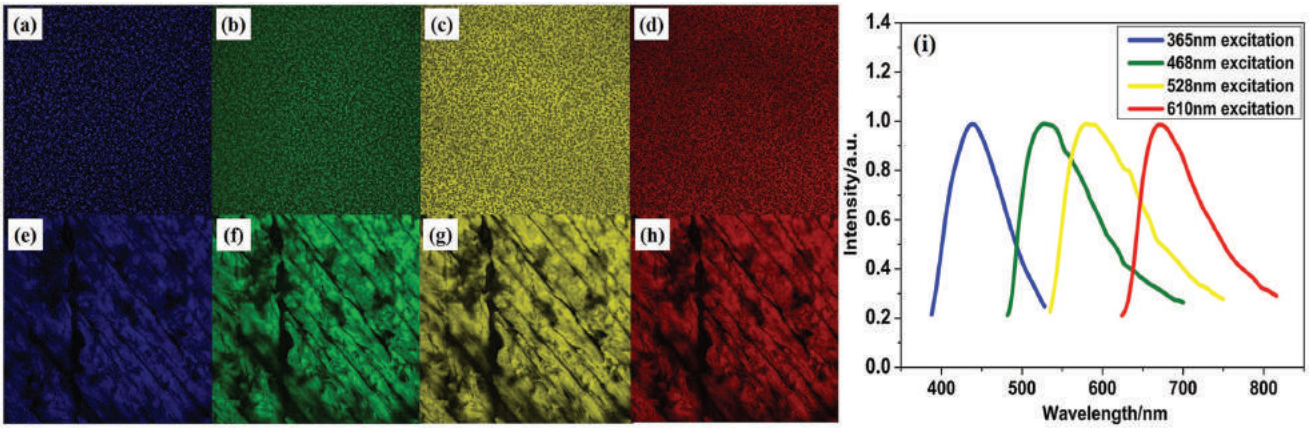

Figure 7. Laser confocal microscope images of PVDF/CQDs (99/1, wt/wt) samples before a–d) and after e–h) high-pressure processing, obtained at ultraviolet a,e), blue b,f), green c,g), and red d,h) excitations, respectively, and typical PL spectra i) of PVDF/CQDs mixtures under different excitations.

CQDs concentration tuning, as well as the combined action of high piezoelectric response and stable multicolor fluorescence in a single composite. This may allow the development of a mechatronics platform for multifunctional self-powered devices, and make the science fiction plots in "Fantastic Voyage" come true in the near future. For example, combining the properties of CQDs and the in situ formed piezoelectric nanostructures, the pressure-crystallized hybrid composites may permit niche applications in the next-generation self-powered multicolor bioimaging micro/nanorobotics by efficiently converting the mechanical and hydraulic energy prevalent in living organisms, such as body movement, muscle stretching, blood vessel contraction, body fluid, and blood flow, into electrical energy.[29–34] The micro/nanometer sized PVDF/CQDs may be further functionalized on its surface, and then bioconjugated to a specific antibody, enabling the self-powered micro/nanorobotic specifically bind to cancer cells with high efficiency, thereby providing new possibilities for various applications in targeted and visualized biomedical sensing, diagnosis, and cell imaging.[34]

Flexible NGs, based on the coupling of flexible electronics and piezoelectric, triboelectric and hybrid NGs, have been extensively studied, due mainly to their great potential for driving low power personal electronics and self-powered sensors.[35,36] As one of the limited known piezoelectric classes of polymers, PVDF and its composites showed more advantageous properties such as flexibility, adequate mechanical strength, processing easiness, and high chemical resistance than their inorganic counterparts, which has already been proven in many references.[35,36] The energy harvesting perfomance, evaluated at varied load amplitudes and frequencies (Figures 3 and 4 and Figures S1 and S2), revealed significantly enhanced piezoelectric efficiency in poling-free PVDF/CQDs composite materials compared to intrinsic PVDF piezoelectric conversion efficiency. Particularly, the maximum open-circuit voltage output density of the durable PVDF/CQDs nanogenerator, without any treatment of electrical poling, reached 19.2 V cm^{-2}, surpassing that of state-of-the-art piezopolymers reported to date. This suggests the PVDF/CQDs composites are qualified for efficiently collecting of the kinetic energy with aperiodic and irregular forms in practical applications.[36] Moreover, the high stable multicolor PL in the PVDF/GQDs composite was demonstrated (Figure 7). Its fluorescence properties were retained even after the endurance for a rigorous treatment at high pressure and high temperature. This confirmed the composite might also find its applications in severe conditions for environmental monitoring.[22,23] In these ways, the as-developed PVDF/CQDs may diversify niche applications in self-powered autonomous optoelectronic devices operated in complex and volatile harsh environments.[36]

3. Conclusion

In summary, we have successfully demonstrated the design and fabrication of a novel PVDF/CQDs-based poling-free self-powered hybrid composite, prepared through solution casting and subsequent high-pressure crystallization. Depending on their loading concentrations, the CQDs induced the self-assembly of PVDF macromolecular chains into various unique piezoelectric nanostructures at high pressure, including 3D nanosheet arrays, 1D nanometer small stick, and 1D nanowires, respectively. The in situ formed nanostructures with special morphologies significantly enhanced the efficiency of mechanical-to-electrical conversion. Without any electrical poling, the maximum short-circuit current output density of the PVDF/CQDs composite reached 550 nA cm^{-2}, open-circuit voltage output density up to 19.2 V cm^{-2}, both remarkably exceeding that of pure PVDF. The as-prepared PVDF/CQDs showed excellent performance in kinetic energy harvesting, and due to its flexible form their size and way of employment can be scaled up from nano- and microdevices to large area systems depending on the application. At the same time, due to the special properties of CQDs, the material exhibited strong and stable multicolor photoluminescent behavior. We believe the work shall make considerable contributions to the development of environmental friendly self-powered devices, and the material system has great potential in the field of biosensors, cell imaging, and autonomous monitoring devices.

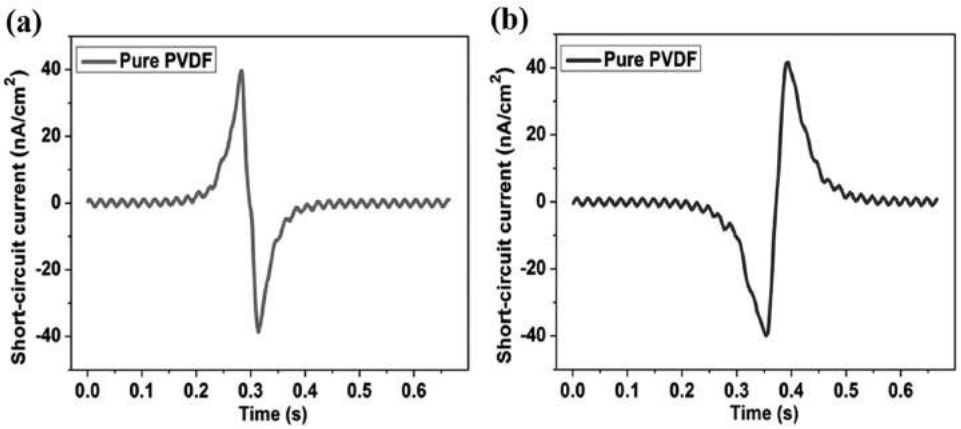

Figure 8. Short-circuit current output density for the pure PVDF when it is a) forward connected and b) reverse connected to the measurement system, respectively. Crystallization conditions: 400 MPa, 260 °C for 10 min.

4. Experimental Section

CQDs were supplied by Nanjing Newcastle New Materials Co., Ltd., with excitation wavelength of 350 nm, and emission wavelength of 440 nm. PVDF powder, commercial-grade Solef 6010, was purchased from Solvay Co., Ltd., Belgium, with average molecular weight of 322 000 g mol^{-1}. Analytical grade *N*,*N*-dimethylformamide (DMF) was provided by Chengdu Kelong Chemical Co., Ltd, and used as received. PVDF solution was prepared by dissolving PVDF powder into DMF, stirring at 60 °C, and then different contents of CQDs were added into the PVDF/DMF solution, followed by 4 h mechanical stirring; homogeneously dispersed PVDF/CQDs solution was coated on a glass substrate and dried in a vacuum oven at 70 °C for 6 h to remove the DMF solvent. Finally, the dried blend films were detached and pelletized for the following high-pressure crystallization. Prior to the high-pressure treatment, transmission electron microscopy (TEM) was employed to observe the morphology and dispersion of the CQDs in PVDF matrix, and the results showed they achieved an overall good dispersion in the composite films with different component ratios (Figure S3, Supporting Information).

High-pressure experiments for the PVDF/CQDs composite, prepared by the solution casting approach stated above, were conducted with a prototype self-made piston-cylinder apparatus. After loading the PVDF/CQDs granules, the temperature was increased to 200 °C to melt the composite. Then a low pressure (150 MPa) was applied, and the temperature was raised to 200 °C. After equilibrium was established, the pressure was further raised to 400 MPa. These samples were kept under these conditions for 10 min, and then quenched down to ambient conditions. The PVDF/CQDs specimens, with a consistent column aspect, 8.04 mm in diameter and 0.50 mm in thickness, were prepared by varying CQDs loadings. For reference, a pure PVDF sample was also prepared under the same treatment.

TEM observations were performed with a JEOL JEM-2100F apparatus. Laser scanning confocal microscope (LSCM) detections were conducted with a KEYENCE VK-9700 apparatus. PL spectra were obtained at room temperature using a FLS980 spectrometer (Edinburgh Instruments) with a 450W Xenon lamp. DSC measurements were conducted at atmospheric pressure using a TA-Q20 instrument. WAXD results were obtained at room temperature with a DX-1000 diffractometer. ATR-FTIR data were obtained using a Nicolet 5700 spectrometer. Thereinto, the fraction of diversiform crystals in the samples were quantified by applying the following formulas[37]:

$$F_{(\beta,\gamma)} = \frac{A_{840}}{A_{840} + 1.26 \times A_{765}} \times X_c \quad (1)$$

$$F_{(\beta)} = \frac{A_{1280}}{A_{1280} + A_{1234}} \times F_{(\beta,\gamma)} \quad (2)$$

$$F_{(\gamma)} = F_{(\beta,\gamma)} - F_{(\beta)} \quad (3)$$

$$F_{(\alpha)} = X_c - F_{(\beta,\gamma)} \quad (4)$$

where A_{840}, A_{765}, A_{1280}, and A_{1234} represent peak areas at 765 (α phase), 840 (β and γ phase), 1280 (β phase), and 1234 cm^{-1} (γ phase) in FTIR spectrum, respectively; and X_c is the crystallinity of the sample. After the WAXD and ATR-FTIR characterizations, the sample surfaces were etched using a method modified from that developed by Vaughan,[38] and then coated with gold for SEM observations using a JSM-6330F apparatus.

The energy harvesting performance of the samples, without any electrical poling treatment, was evaluated by a periodic impacting test, with an experimental setup described in a recent publication.[11] A NTIAG HS01-37 × 166 linear motor was used as the impact source, and the simultaneously generated open-circuit voltage and short-circuit current were collected with a Keithley 6514 system electrometer and a Stanford Research SR570 low-noise current preamplifier, respectively. To confirm the collected electrical signals were right-down from the piezoelectric generator rather than from the testing system, the anode wire was exchanged with the cathode wire, and switching polarity tests were conducted for the PVDF-based generator. As expected, the wave patterns appeared in the opposite direction, whereas there was little difference between the electrical output value (**Figure 8**).

Supporting Information

Supporting Information is available from the Wiley Online Library or from the author.

Acknowledgements

S.M. and L.J. contributed equally to this work. This work was supported by the National Natural Science Foundation of China (No. 51373139), Sichuan Science and Technology Program (No. 2018JY0166), and Technological Projects for Distinguished Young Scholars of Sichuan Province (No.2015JQ0013). The authors extended their gratitude to Professor Yajiang Huang (Sichuan University) for valuable discussions and Dr. Fengjun Chun (Southwest Jiaotong Univeristy) for helps in performing the PL tests.

Conflict of Interest

The authors declare no conflict of interest.

Keywords

composite materials, electro-optical materials, flexible electronics, luminescence, quantum dots

Received: April 17, 2018
Revised: June 18, 2018
Published online:

[1] a) B. Saravanakumar, S. Soyoon, S. J. Kim, *ACS Appl. Mater. Interfaces* **2014**, *6*, 13716; b) B. Saravanakumar, K. Thiyagarajan, N. R. Alluri, S. S. Yoon, K. Taehyun, Z. H. Lin, S. J. Kim, *Carbon* **2015**, *84*, 56.

[2] a) X. J. Zhao, J. J. Tian, S. Y. Kuang, H. Ouyang, L. Yan, Z. L. Wang, Z. Li, G. Zhu, *Adv. Mater. Interfaces* **2016**, *3*, 1600187; b) X. Y. Wei, L. P. Liu, H. L. Wang, S. Y. Kuang, X. X. Zhu, Z. L. Wang, Y. H. Zhang, G. Zhu, *Adv. Mater. Interfaces* **2018**, *5*, 1701063.

[3] a) X. Wang, J. Song, J. Liu, Z. L. Wang, *Science* **2007**, *316*, 102; b) Y. Qin, X. Wang, Z. L. Wang, *Nature* **2008**, *451*, 809.

[4] a) S. N. Cha, J. S. Seo, S. M. Kim, J. H. Kim, Y. J. Park, S. W. Kim, J. M. Kim, *Adv. Mater.* **2010**, *22*, 4726; b) J. H. Lee, K. Y. Lee, B. Kumar, T. N. Tien, N. E. Lee, S. W. Kim, *Energy Environ. Sci.* **2013**, *6*, 169; c) J. H. Lee, H. J. Yoon, T. Y. Kim, M. K. Cupta, J. H. Lee, W. Seung, H. Ryu, S. W. Kim, *Adv. Funct. Mater.* **2015**, *25*, 3276.

[5] a) C. Emmanouilidis, C. Riziotis, in *Engineering Asset Management - Systems, Professional Practices and Certification, Lecture Notes in Mechanical Engineering* (Eds: P. W. Tse, J. Mathew, K. Wong, R. Lam, C. N. Ko), Springer, Cham **2015**, pp. 1389–1400; b) A. El Sachat, A. Meristoudi, C. Markos, A. Sakellariou, A. Papadopoulos, S. Katsikas, C. Riziotis, *Sensors* **2017**, *17*, 568.

[6] D. Pan, F. Dai, H. Li, *Compos. Sci. Technol.* **2015**, *119*, 34.

[7] Z. H. Lin, Y. Yang, J. M. Wu, Y. Liu, F. Zhang, Z. L. Wang, *J. Phys. Chem. Lett.* **2012**, *3*, 3599.

[8] a) D. Karanth, H. Fu, *Phys. Rev. B* **2005**, *72*, 064116; b) Z. L. Wang, J. Song, *Science* **2006**, *312*, 242; c) Q. Yang, X. Guo, W. Wang, Y. Zhang, S. Xu, D. H. Lien, Z. L. Wang, *ACS Nano* **2010**, *4*, 6285.

[9] a) G. Wang, Y. Xi, H. Xuan, R. Liu, X. Chen, L. Cheng, *Nano Energy* **2015**, *18*, 28; b) H. J. Kim, J. H. Kim, K. W. Jun, J. H. Kim, W. C. Seung, O. H. Kwon, J. Y. Park, S. W. Kim, I. K. Oh, *Adv. Energy Mater.* **2016**, *6*, 1502329.

[10] S. Chen, X. Li, K. Yao, F. E. H. Tay, A. Kumar, K. Zeng, *Polymer* **2012**, *53*, 1404.

[11] C. Lu, L. Zhang, C. W. Xu, Z. Z. Yin, S. B. Zhou, J. X. Wang, R. Huang, X. Q. Zhou, C. L. Zhang, W. Q. Yang, J. Lu, *RSC Adv.* **2016**, *6*, 67400.

[12] J. C. Wang, J. L. Wu, W. Xu, Q. Zhang, Q. Fu, *Compos. Sci. Technol.* **2014**, *91*, 1.

[13] a) Y. Hu, Y. Zhang, C. Xu, G. Zhu, Z. L. Wang, *Nano Lett.* **2010**, *10*, 5025; b) Z. Li, Z. L. Wang, *Adv. Mater.* **2011**, *23*, 84; c) C. L. Sun, J. Shi, D. J. Bayerl, X. D. Wang, *Energy Environ. Sci.* **2011**, *4*, 4508; d) T. Sharma, S. S. Je, B. Gill, X. John, J. Zhang, *Sens. Actuators, A* **2012**, *177*, 87.

[14] Y. Liu, Y. Hu, J. Zhao, G. Wu, X. M. Tao, W. Chen, *Small* **2016**, *12*, 5074.

[15] F. J. Zhang, Y. P. Zang, D. Z. Huang, C. A. Di, D. B. Zhu, *Nat. Commun.* **2015**, *6*, 8356.

[16] a) Y. Qin, X. D. Wang, Z. L. Wang, *Nature* **2008**, *451*, 809; b) Z. L. Wang, *ACS Nano* **2013**, *7*, 9533.

[17] a) J. I. Scheinbeim, S. C. Mathur, B. A. Newman, *Macromolecules* **1986**, *50*, 6095; b) J. F. Zheng, A. H. He, J. X. Li, C. C. Han, *Macromol. Rapid Commun.* **2007**, *28*, 2159; c) R. P. Vijayakumar, D. V. Khakhar, A. Misra, *J. Appl. Polym. Sci.* **2010**, *117*, 3491.

[18] P. Tian, C. Xu, H. Huang, X. Chen, L. Zhao, J. Lyu, *Gut* **2016**, *65*, A231.

[19] C. W. Xu, L. Zhang, Y. L. Xu, Z. Z. Yin, Q. Chen, S. Y. Ma, H. H. Zhang, R. Huang, C. L. Zhang, L. Jin, W. Q. Yang, J. Lu, *J. Mater. Chem. A* **2017**, *5*, 189.

[20] a) M. G. Bawendi, M. L. Steigerwald, L. E. Brus, *Annu. Rev. Phys. Chem.* **1990**, *41*, 477; b) K. A. S. Fernando, S. Sahu, Y. Liu, W. K. Lewis, E. A. Guliants, A. Jafariyan, P. Wang, C. E. Bunker, Y. P. Sun, *ACS Appl. Mater. Interfaces* **2015**, *7*, 8363.

[21] a) X. Liu, H. Jiang, J. Lei, H. X. Ju, *Anal. Chem.* **2007**, *79*, 8055; b) Y. Shan, J. J. Xu, H. Y. Chen, *Chem. Commun.* **2010**, *46*, 5079; c) G. X. Liang, L. L. Li, H. Y. Liu, J. R. Zhang, C. Burda, J. J. Zhu, *Chem. Commun.* **2010**, *46*, 2974; d) Y. H. Xu, J. Q. Liu, C. L. Gao, E. Wang, *Electrochem. Commun.* **2014**, *48*, 151.

[22] a) X. T. Zheng, A. Ananthanarayanan, K. Q. Luo, P. Chen, *Small* **2015**, *11*, 1620; b) S. Gogoi, M. Kumar, B. B. Mandal, N. Karak, *Compos. Sci. Technol.* **2015**, *118*, 39; c) S. Y. Lim, W. Shen, Z. Gao, *Chem. Soc. Rev.* **2015**, *44*, 362; d) H. Wang, C. Sun, X. R. Chen, Y. Zhang, V. L. Colvin, Q. Rice, J. Seo, S. Y. Feng, S. N. Wang, W. W. Yu, *Nanoscale* **2017**, *9*, 1909.

[23] a) S. Liu, J. Tian, L. Wang, Y. Zhang, X. Qin, Y. Luo, A. M. Asiri, A. O. Alyoubi, X. Sun, *Adv. Mater.* **2012**, *24*, 2037; b) S. Y. Park, H. U. Lee, Y. C. Lee, S. Choi, D. H. Cho, H. S. Kim, S. Bang, S. Seo, S. Bang, S. Seo, S. C. Lee, J. Won, B. C. Son, M. Yang, J. Lee, *Sci. Rep.* **2015**, *5*, 12420.

[24] a) M. Favaro, S. Leonardi, C. Valero-vidal, S. Nappini, M. Hanzlik, S. Agnoli, J. Kunze-Liebhaeuser, G. Granozzi, *Adv. Mater. Interfaces* **2015**, *2*, 1400462; b) D. Wang, J. Y. Liu, J. F. Chen, L. M. Dai, *Adv. Mater. Interfaces* **2016**, *3*, 1500439; c) Y. Li, W. S. Zhang, L. Zhang, J. F. Li, Z. Q. Su, G. Wei, *Adv. Mater. Interfaces* **2017**, *4*, 1600895; d) Y. L. Ying, P. He, M. J. Wei, G. Q. Ding, X. S. Peng, *Adv. Mater. Interfaces* **2017**, *4*, 1700209.

[25] K. S. Ramadan, D. Sameoto, S. Evoy, *Smart Mater. Struct.* **2014**, *23*, 033001.

[26] J. Lu, R. Huang, L. B. Li, J. B. Luo, *Macromol. Rapid Commun.* **2005**, *26*, 1478.

[27] a) W. Yang, W. T. Duan, S. Ahmed, T. E. Mallouk, A. Sen, *Nano Today* **2013**, *8*, 531; b) W. Gao, J. Wang, *ACS Nano* **2014**, *8*, 3170; c) X. Ma, A. Jannasch, U.-R. Albrecht, K. Hahn, A. Miguel-López, E. Schäffer, S. Sánchez, *Nano Lett.* **2015**, *15*, 7043; d) M. Hansen-Bruhn, B. E.-F. de Ávila, M. Beltrán-Gastélum, J. Zhao, D. E. Ramírez-Herrera, P. Angsantikul, K. Vesterager Gothelf, L. F. Zhang, J. Wang, *Angew. Chem., Int. Ed.* **2018**, *57*, 2657; e) S. Hermanova, M. Pumera, *Nanoscale* **2018**, *10*, 7332.

[28] a) J. Z. Wang, Z. Xiong, X. J. Zhan, B. H. Dai, J. Zheng, J. Liu, J. Y. Tang, *Adv. Mater.* **2017**, *29*, 1701451; b) J. K. Qin, G. Qiu, J. Jian, H. Zhou, L. M. Yang, A. Charnas, D. Y. Zemlyanov, C. Y. Xu, X. F. Xu, W. Z. Wu, H. Y. Wang, P. D. Ye, *ACS Nano* **2017**, *11*, 10222; c) L. L. Wang, H. H. Shao, W. J. Wang, J. R. Zhang, J. J. Zhu, *Nano Energy* **2018**, *44*, 95.

[29] a) Z. L. Wang, W. Z. Wu, *Angew. Chem., Int. Ed.* **2012**, *51*, 11700; b) Q. Zheng, B. J. Shi, Z. Li, Z. L. Wang, *Adv. Sci.* **2017**, *4*, 1700029. c) M. A. P. Mahmud, N. Huda, S. H. Farjana, M. Asadnia, C. Lang, *Adv. Energy Mater.* **2018**, *8*, 1701210.

[30] L. W. Jang, J. Lee, M. E. Razu, E. C. Jensen, J. Kim, *IEEE Trans. Nanobiosci.* **2015**, *14*, 841.

[31] I. Posadas, S. Monteagudo, V. Ceña, *Nanomedicine (London, U. K.)* **2016**, *11*, 833.

[32] a) A. Pramanik, A. Vangara, B. P. V. Nellore, S. S. Sinha, S. R. Chavva, S. Jones, P. C. Ray, *ACS Appl. Mater. Interfaces* **2016**, *8*, 15076; b) M. J. Sun, B. Sun, Y. Liu, Q. D. Shen, S. J. Jiang, *Sci. Rep.*

2016, *6*, 22368; c) M. Zhang, W. T. Wang, P. Yuan, C. Chi, J. Zhang, N. L. Zhou, *Chem. Eng. J.* **2017**, *330*, 1137; d) S. Huang, E. L. Yang, Y. Liu, J. D. Yao, W. Su, Q. Xiao, *Sens. Actuators, B* **2018**, *265*, 326.

[33] a) S. Li, Z. Guo, R. Feng, Y. Zhang, W. Xue, Z. H. Liu, *RSC Adv.* **2017**, *7*, 4975; b) J. Y. Chen, M. Y. Liu, Q. Huang, L. Huang, H. Y. Huang, F. J. Deng, Y. Q. Wen, J. W. Tian, X. Y. Zhang, Y. Wei, *Chem. Eng. J.* **2018**, *337*, 82; c) J. J. Gu, X. L. Li, D. H. Hu, Y. F. Liu, G. Y. Zhang, X. D. Jia, W. Y. Huang, K. Xi, *RSC Adv.* **2018**, *8*, 12556.

[34] M. Yuksel, D. G. Colak, M. Akin, I. Cianga, M. Kukut, E. I. Medine, M. Can, S. Sakarya, P. Unak, S. Timur, Y. Yagci, *Biomacromolecules* **2012**, *13*, 2680.

[35] a) D. Shah, P. Maiti, E. Gunn, D. F. Schmidt, D. D. Jiang, C. A. Batt, E. P. Giannelis, *Adv. Mater.* **2004**, *16*, 1173; b) F. R. Fan, W. Tang, Z. L. Wang, *Adv. Mater.* **2016**, *28*, 4283.

[36] L. Jin, S. Y. Ma, W. L. Deng, C. Yan, T. Yang, X. Chu, G. Tian, D. Xiong, J. Lu, W. Q. Yang, *Nano Energy* **2018**, *50*, 632.

[37] a) S. J. Kang, Y. J. Park, I. Bae, K. J. Kim, H. C. Kim, S. Bauer, E. L. Thomas, C. Park, *Adv. Funct. Mater.* **2009**, *19*, 2812; b) N. Jia, Q. Xing, X. Liu, J. Sun, G. M. Xia, W. Huang, R. Song, *J. Colloid Interface Sci.* **2015**, *453*, 169.

[38] A. S. Vaughan, *J. Mater. Sci.* **1993**, *28*, 1805.

